# Interaction regimes for oppositely charged plates with multivalent counterions

Fabien Paillusson

*Department of Chemistry, University of Cambridge, Lensfield Road, Cambridge CB2 1EW, United Kingdom*

Emmanuel Trizac

*Laboratoire de Physique Théorique et Modèles Statistiques, Unité Mixte de Recherche No. 8626 associée au Centre National de la Recherche Scientifique, Université Paris-Sud, F-91405 Orsay, France*

Within a mean-field treatment of the interaction between two oppositely charged plates in a salt-free solution, the distance at which a transition from an attractive to a repulsive regime appears can be computed analytically. The mean-field description, however, breaks down under strong Coulombic couplings, which can be achieved at room temperature with multivalent counterions and highly charged surfaces. Making use of the contact theorem and simple physical arguments, we propose explicit expressions for the equation of state in several situations at short distances. The possibility of Bjerrum pair formation is addressed and is shown to have profound consequences on the interactions. To complete the picture, we consider the large-distance limit, from which schematic phase diagram discriminating attractive from repulsive regions can be proposed.

## I. INTRODUCTION

Although it has been less studied than its like-charge counterpart [1–3], the behavior of two interacting oppositely charged mesoscopic bodies in solution is of importance in various contexts, including colloid physics [4–8], biochemistry-related experiment interpretations [9,10], drug design [11], and structural biology [12]. The simple system of two charged plates with opposite uniform surface charges represents a model of choice that enables one to get analytical results in some limits and furthermore provides a starting point to estimate the interaction energy between two colloids of various geometries [13,14]. It has been shown that opposite-charge repulsion could occur within a mean-field (MF) treatment [15,16]. The physical origin of such a repulsion has been identified as twofold: a Born repulsion due to short-range polarization effects when the solvent has a dielectric constant that significantly exceeds those of the macromolecules [4,17] and an osmotic repulsion resulting from the trapping of the counterions that ensure electroneutrality between the unequally charged plates [18,19]. Within a mean-field approach for $q$:$q$ symmetric solutions (with $q = 1$), it has also been emphasized recently that the osmotic repulsion may explain how the proteins' shape determines their interaction with DNA [20]: The essential physics of the ion-mediated interaction between these biomolecules is well captured by a simple two-plate model, which opens the way to analytical estimates of the location and depth of the corresponding energy well.

In salt-free solutions with spherical counterions of size $b$, the threshold distance $D_{MF}^* = h_{MF}^* - b$ at which the electrostatic attraction is dominated by the osmotic repulsion for two plates bearing uniform surface charges $\sigma_1 e$ and $\sigma_2 e$ (with $\sigma_1 \sigma_2 < 0$) is simply given, within the mean field, by the difference of their respective Gouy-Chapman lengths: $D_{MF}^* = |\mu_1 - \mu_2|$ [19]. These quantities read $\mu_{1,2} = (2\pi q l_B |\sigma_{1,2}|)^{-1}$, where $l_B = e^2/4\pi \varepsilon k_B T$ is the Bjerrum length (about 0.7 nm in water at room temperature), which is defined using temperature $T$ and solvent permittivity $\varepsilon$. Relying on the Poisson-Boltzmann MF approximation, the previous result only holds provided

the Coulombic coupling between counterions is not too large. More specifically, this means that the two coupling parameters $\Xi_1$ and $\Xi_2$, defined as $\Xi_i = 2\pi l_B^2 q^3 |\sigma_i|$, should both be small [2,21]. However, in cases of practical interest with multivalent counterions, the coupling parameter may be large; for instance, converting the charge of double-stranded DNA into an equivalent surface charge, one finds $\Xi \simeq 23$ in water at room temperature with divalent ions ($q = 2$) and $\Xi \simeq 76$ with $q = 3$ [22]. In this paper our goal is therefore to study the fate of the attraction-repulsion transition for oppositely charged interfaces under strong Coulombic coupling (large-$\Xi$ limit).

For the following discussion it is instructive to recall the essential features of a single strongly coupled planar double layer without added salt (i.e., counterions only ensure electroneutrality) [21–32]. Irrespective of the value of $\Xi$ (from mean-field to strong coupling), the typical distance that counterions may explore away from the charged wall is given by the Gouy-Chapman length $\mu$ defined above. At large-$\Xi$ values, the counterions form a strongly modulated liquid (if not a true crystal at asymptotically large $\Xi$), with a typical distance between ions measured by $a_\perp = \sqrt{q/\pi\sigma}$ [23], as required by electroneutrality ($\sigma \pi a_\perp^2 \simeq q$). It therefore appears that $\mu \ll a_\perp$ when $\Xi \gg 1$, where $a_\perp$ measures the size of the correlation hole around each ion. As a consequence, the counterions, which form a strongly correlated liquid parallel to the plate, effectively decouple in the direction perpendicular to the plate and the leading-order profile in the strong-coupling expansion is given by the interactions of individual counterions with the confining charged interface [21–32]: This single-particle picture simply yields a leading exponential counterion density profile, with a characteristic length $\mu$. Counterion interactions contribute to the subleading terms [31] and will not be addressed here: We shall restrict the discussion to the easily attainable gains of the single-particle viewpoint, which provides the dominant strong-coupling behavior. We also stress that again for large $\Xi$, we have not only $\mu \ll a_\perp$ but also $a_\perp \ll q^2 l_B$. More precisely, it is useful to keep in
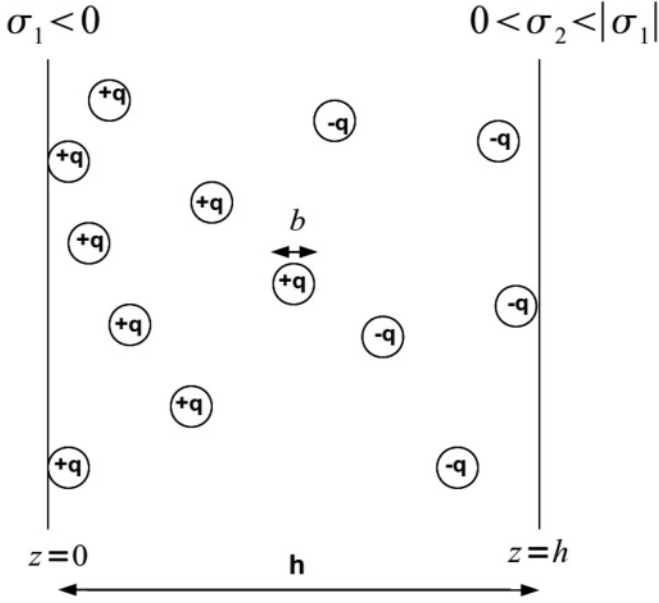
FIG. 1. Schematic view of the two-plate system. Microions are hard spheres of diameter $b$ with charges $qe$ and $-qe$. The width of the slab between the plates is denoted by $h$ and we define $D$ as $h-b$.

mind the relations

$$\frac{a_\perp}{\mu\sqrt{2}} = \frac{q^2 l_B \sqrt{2}}{a_\perp} = \sqrt{\frac{q^2 l_B}{\mu}} = \sqrt{\Xi}, \qquad (1)$$

where the numerical constants are immaterial.

In the following we shall consider two uniformly charged plates 1 and 2, with respective charge densities $\sigma_1 < 0$ and $0 < \sigma_2 < |\sigma_1|$. Plate 1 is neutralized by counterions of valency $q > 0$ while $-q$ counterions neutralize plate 2. The corresponding microions remain in the gap of width $h$ between the plates to ensure global electroneutrality (see Fig. 1). Our goal is to characterize the strong-coupling regimes and to infer the equation of state at short distances from the knowledge of ionic density profiles, making repeated use of the contact value theorem [33,34], which will be recalled in due time. Several situations will be worked out, depending on the formation of $+q/-q$ Bjerrum pairs between oppositely charged microions. In addition to $\Xi_1$ and $\Xi_2$, the physics of the problem is thus ruled by another coupling parameter $\Gamma$, to be introduced in Sec. II A, which quantifies the tendency to form $+q/-q$ pairs. This short-range study is developed in Secs. II B and II C. It will be complemented by a large-distance analysis in Sec. II D, from which a tentative phase diagram, which allows one to discriminate repulsive from attractive regions, will be put forth. Conclusions will be drawn and the possible relevance of our approach to weak couplings will be discussed in Sec. III.

## II. STRONG-COUPLING APPROACH FOR OPPOSITELY CHARGED PLATES

### A. Crowding versus pairing

Whereas previous works pertaining to the strong-coupling limit have been mostly performed in the limit of point counterions, in some cases it is possible to transpose the results
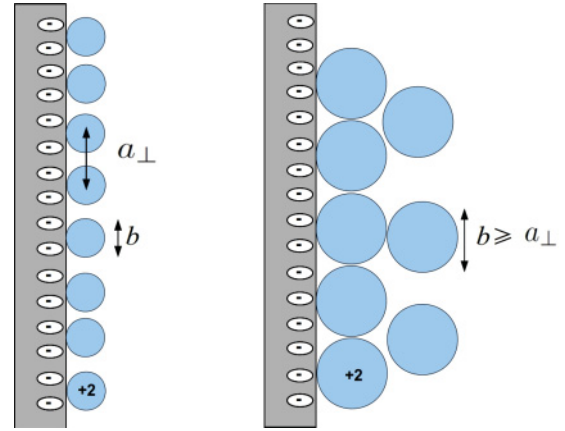


FIG. 2. (Color online) Two strongly coupled double layers in different crowding regimes. The left-hand-side plot shows the uncrowded situation where the finite ionic size does not perturb the point-counterion predictions while the right-hand-side plot is for a case where hard core effects lead to crowding, with bilayers or multilayers of counterions in the vicinity of the plate. For this example to be meaningful, we set $q = 2$ for the valency of the counterions.

to the case of finite-size ions, essentially by taking $b/2$ (the ionic radius) as the ion-plate distance of closest approach. For a single plate, the density profiles in the two cases are therefore identical up to a coordinate shift $z \to z - b/2$, where $z$ denotes the distance to the plate. Likewise, in the two-plate problem, the plate-plate distance of closest approach is $b$. More precisely, the $b = 0$ and $b \neq 0$ cases coincide provided packing effects are negligible (see Fig. 2, left) while increasing ionic size $b$ necessarily leads to a situation where $b$ becomes of the order of $a_\perp$, so that the double layer can no longer accommodate a monolayer of counterions (see Fig. 2, right). Understanding the behavior of strongly coupled and crowded double layers is an open problem that lies beyond the scope of the present work, so we will restrict our study to the cases where $b < a_\perp$, i.e., to not-too-big microions. This requirement should be enforced for both plates: $b < a_\perp^{(1),(2)}$.

In addition to crowding, microion pairing may take place in the two-plate problem [2,35] (see Fig. 3). The tendency for $q$ and $-q$ microions to form neutral pairs at $T \neq 0$ is quantified by the ratio between the direct electrostatic interaction at close contact and $k_B T$, i.e., $\Gamma = q^2 l_B / b$. Interestingly, keeping in mind the no-crowding condition sketched above ($b < a_\perp^{(1),(2)}$), we get the inequality $2\Gamma^2 > \Xi$ [where $\Xi = \max(\Xi_1, \Xi_2) = \Xi_1$], so that the possible values $\Gamma$ can take are bounded from below by $\sqrt{\Xi/2}$. Consequently, strongly coupled uncrowded double layers lead to the important formation of Bjerrum pairs (large $\Gamma$). We nevertheless start by considering the rather narrow region where $3 \lesssim \sqrt{\Xi/2} < \Gamma < 10$ in which pair formation can be neglected. The above constraint translates into $20 < \Xi < 200$, where $\Xi$ is large enough to allow for a strong-coupling analysis in due form to unveil the main features. A more quantitative description presumably requires, especially at the smaller-$\Xi$ values involved, an intermediate approach interpolating between the mean-field and strong-coupling limits [36–39].
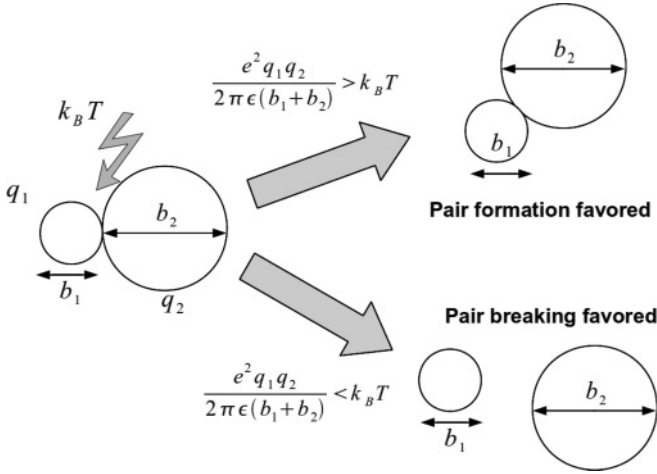
FIG. 3. Pair-breaking–pair-formation mechanism. Starting from a contact configuration for two ions of opposite charges $q_1 e$ and $-q_2 e$ on the left-hand side, the tendency to remain in this configuration or, on the contrary, to break the pair is given by comparing the electrostatic loss to the thermal energy.

### B. Small separation distances without pair formation

We define in the subsequent analysis $D$ as the shifted distance between the plates: $D = h - b$. The first situation addressed is that in which Bjerrum pair formation can be neglected, which is the assumption made in Ref. [25]. Under strong coupling, if $D < a_\perp^{(1)}$ (which implies that $D < a_\perp^{(2)}$ since $\sigma_2 < |\sigma_1|$), the single-particle picture where each microion interacts with both plates only and not with its fellow microions is valid. A tagged microion experiences an electric field $-2\pi(|\sigma_1| + \sigma_2)\hat{z}/\varepsilon$, where $\hat{z}$ is a unit vector along the $z$ direction, hence a linear potential in $z$. The corresponding number densities $n_+(z)$ and $n_-(z)$ for both $q$ and $-q$ species then follow a simple Boltzmann law

$$n_\pm(z) = n_\pm^{(0)} e^{\mp \tilde{z}}, \tag{2}$$

where $n_+^{(0)}$ and $n_-^{(0)}$ are two normalization constants and we introduced the reduced distance to plate 1,

$$\tilde{z} = z/\lambda \quad \text{with} \quad \frac{1}{\lambda} = \frac{1}{\mu_1} + \frac{1}{\mu_2}. \tag{3}$$

The two factors $n_\pm^{(0)}$ can be determined from the electroneutrality conditions

$$q \int_{b/2}^{h-b/2} dz\, n_+^{(0)} = |\sigma_1|, \tag{4}$$

$$q \int_{b/2}^{h-b/2} dz\, n_-^{(0)} = \sigma_2, \tag{5}$$

so that

$$n_+(\tilde{z}) = \frac{|\sigma_1| e^{\tilde{b}/2 - \tilde{z}}}{q\lambda(1 - e^{\tilde{b} - \tilde{h}})}, \tag{6}$$

$$n_-(\tilde{z}) = \frac{\sigma_2 e^{-\tilde{b}/2 + \tilde{z}}}{q\lambda(e^{-\tilde{b} + \tilde{h}} - 1)}. \tag{7}$$

The expression for the reduced pressure

$$\Pi = 2\pi l_B q^2 \mu_1^2 \beta P = \frac{\beta P}{2\pi\, l_B\, \sigma_1^2} \tag{8}$$

directly follows from the contact value theorem, which yields the pressure $P$ in the form [33,34]

$$P = n_+\left(\frac{b}{2}\right) + n_-\left(\frac{b}{2}\right) - 2\pi l_B \sigma_1^2 \tag{9}$$

$$= n_+\left(h - \frac{b}{2}\right) + n_-\left(h - \frac{b}{2}\right) - 2\pi l_B \sigma_2^2. \tag{10}$$

Consequently, we have

$$\Pi(\tilde{D}) = \zeta \coth\left(\frac{\tilde{D}}{2}\right) + \frac{1}{2}(1 + \zeta^2)\left[\coth\left(\frac{\tilde{D}}{2}\right) - 1\right], \tag{11}$$

where we introduced the charge ratio $\zeta = \sigma_2/|\sigma_1|$. Equation (11) is independent of the plate (1 or 2) where the contact theorem is applied, which provides a consistency test for the argument. In other words, the pressure $P$ is invariant under the change $\zeta \to 1/\zeta$, so the reduced pressure should change according to $\Pi \to \Pi\zeta^{-2}$ when $\zeta \to \zeta^{-1}$. This property can be checked directly in Eq. (11). More importantly, the expression in Eq. (11) is positive for $D > 0$, for all values of the charge ratio (see Fig. 4). Therefore, the interaction between two oppositely charged plates is always repulsive at short distances in this regime. The physical mechanism behind this repulsive behavior is the following. Compared to the large-distance limit where $n_+(b/2) \simeq 2\pi l_B \sigma_1^2$, as follows from Eq. (9) and the fact that both the pressure and $n_-(b/2)$ vanish, bringing the plates at short distances where $D < a_\perp^{(1)}$ enhances the electric field experienced by $q$ microions, which results in the increase of their density at contact with plate 1. Invoking again the contact theorem Eq. (9), the consequence is that $P > 0$. The interactions between $q$ and $-q$ microions could counterbalance this effect, but these interactions have
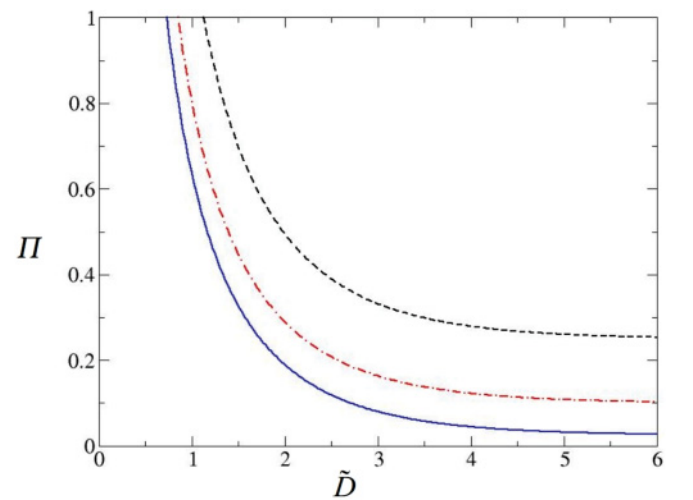


FIG. 4. (Color online) Plot of the reduced pressure following from the short-distance equation of state Eq. (11) as a function of rescaled distance $\tilde{D}$ for several values of $\zeta = \sigma_2/|\sigma_1|$: $\zeta = 0.25$ (dashed line), $\zeta = 0.1$ (dot-dashed line), and $\zeta = 0.025$ (solid line). The short-distance requirement $D < a_\perp^{(1)}$ (the so-called Rouzina-Bloomfield criterion [23]), translates into $\tilde{D} < \Xi^{1/2}$.

been discarded here with the neglect of Bjerrum pair formation. We will see below that $+q/-q$ interactions, when relevant, completely change the phenomenology.

Three remarks are in order here. (i) We see that the reason for observing repulsive behavior (an enhanced electric field acting on a microion within the single-particle picture) is the same as that leading to attraction in the like-charged case (a decreased electric field, with a corresponding decrease of microionic density at contact; this effect is most pronounced in the symmetric case where $\sigma_1 = \sigma_2$, for which the electric field vanishes and the microion densities is uniform in the $z$ direction). (ii) The possibility of attraction under strong coupling reported in Ref. [25] for oppositely charged plates stems from the fact that only one type of microion was considered in Ref. [25]. This results in a smaller amount of counterions (per unit surface) compared to that which is necessary to neutralize the isolated plate, with a concomitant decrease of contact ionic density, which opens the way to a possible attraction. The physical situation considered in Ref. [25] thus differs from the one under study here. (iii) Our finding $P > 0$ relies on the condition $D < a_{\perp}^{(1)}$. At large distances, we should have $P < 0$ since a mean-field scenario is then expected to prevail [24,36,40,41]. We will return to this point in Sec. II D.

### C. Small separation distances with pair formation

We now turn to the case where $1 \ll \sqrt{\Xi/2} < \Gamma$, with a strong tendency for two microions to form a neutral pair. While pair formation is unlikely as long as the two condensed microion layers from each plate do not overlap, it becomes important at smaller separations. By "pair formation" we loosely refer here to the more or less complex structures, or aggregates, that may form from the association of several of individual pairs. Pairs may indeed exist in the form of well-defined entities, but may also self-assemble into chains (see, e.g., Ref. [42]) or into more complex structures (regular or empty crystals) uncovered in a related context in Ref. [43]. The corresponding aggregates are electrically neutral, with the number of Bjerrum pairs involved per unit area limited by the less abundant species of microion, i.e., the counterions of plate 2. Therefore, the aggregate surface density is bounded from above by $\sigma_2/q$. These aggregates coexist with a strongly correlated Wigner-like crystal made up of the remaining majority species. In this work we did not attempt a precise evaluation of the aggregate or pairs' contribution $P_{\text{agg}}$ to the total interplate pressure $P$, but instead we considered two limiting cases where we bound $P_{\text{agg}}$ from below by zero (see Sec. II C 1) and from above by $kT\sigma_2/qD$ (see Sec. II C 2). The latter bound corresponds to a density of aggregates, which are neutral entities, equal to $\sigma_2/qD$, that is, to the maximum mean density of possible pairs. Any self-assembly of the pairs in a more complex architecture leads to a decrease of that density. We now investigate separately these two limiting cases.

#### 1. Without the osmotic contribution from the pairs

With only positive counterions in the system, the typical lateral distance becomes $A_{\perp} = \sqrt{q/\pi(|\sigma_1| - \sigma_2)}$ and for separation distances $D < A_{\perp}$, the single-particle picture holds

and yields the microionic density $n_+(z)$ in a form similar to Eq. (2),

$$n_+(z) = n_+^{(1)} e^{-\tilde{z}}, \tag{12}$$

where $n_+^{(1)}$ is a positive constant. As for $n_+^{(0)}$, the prefactor $n_+^{(1)}$ can be determined using the electroneutrality condition

$$q \int_{b/2}^{h-b/2} dz\, n_+(z) = |\sigma_1| - \sigma_2 \tag{13}$$

and the ion density then reads

$$n_+(z) = \frac{|\sigma_1| - \sigma_2}{q\lambda(1 - e^{\tilde{b}-\tilde{h}})} e^{\tilde{b}/2 - \tilde{z}}. \tag{14}$$

Initially, we do not consider the contribution of Bjerrum pairs to the total pressure (we therefore bound from below the term $P_{\text{agg}}$ by zero). In doing so, the pressure at a given reduced separation distance $\widetilde{D}$ can again be found by means of the contact value theorem, with only one species of microions: $\beta P = n_+(b/2) - 2\pi l_B \sigma_1^2$, so that

$$\Pi(\widetilde{D}) = -\frac{1}{2}(1 + \zeta^2) + \frac{1}{2}(1 - \zeta^2)\coth\left(\frac{\widetilde{D}}{2}\right). \tag{15}$$

We recover the same expression as in Ref. [25] from a mechanical (contact theorem) instead of energy route. Unlike Eqs. (11) and (15) does not have a definite sign and as a consequence the interaction is attractive at large distances: There exists a threshold

$$D_0^* = 2\lambda \ln(|\sigma_1|/\sigma_2) \tag{16}$$

below which the interaction becomes repulsive ($\Pi > 0$) (see Fig. 5). We note from Eq. (16) that attraction prevails until $D \to 0$ when $\sigma_2 \to |\sigma_1|$ and we add that as long as microions (even a small amount) remain between the plates as required by electroneutrality, the corresponding entropy cost for confinement makes the pressure diverge (hence positivity) for $D \to 0$. Only for $\zeta = 1$, i.e., $\sigma_2 = -\sigma_1$, would the microion total density vanish, which leaves two oppositely charged plates interacting without any screening. In that specific case the interaction is obviously attractive until close contact $h = 0$. In contrast, in the large-$\widetilde{D}$ limit, with the requirement
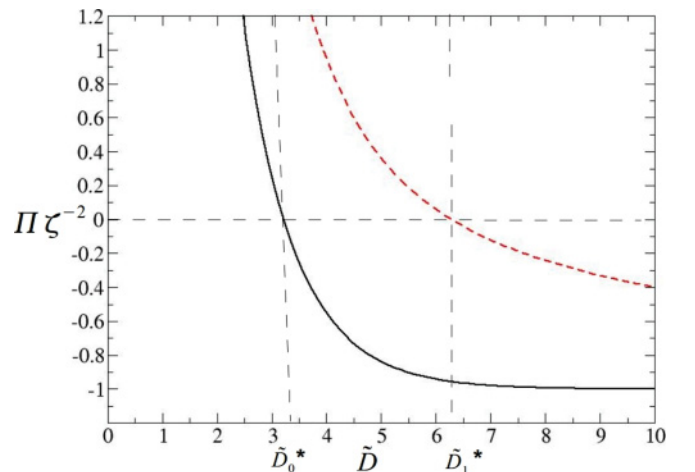


FIG. 5. (Color online) Pressure curves from Eqs. (15) (solid line) and (17) (dashed line) for $\zeta = 0.2$.

$D < A_\perp$ nevertheless enforced, and for any value of $\zeta$ one can immediately find the pressure from the contact theorem applied at plate 2: For large $\widetilde{D}$ the positive microions are expelled from the vicinity of the positive plate, which means that the contact density $n_+(h - d/2)$ vanishes and $\beta P \to -2\pi l_B \sigma_2^2$. In terms of rescaled pressure, we then have $\Pi \to -\zeta^2$, which is indeed observed in Fig. 5.

### 2. With the osmotic contribution from the pairs

We now include the pairs' contribution to the equation of state through the upper bound $\sigma_2/qD$ alluded to above. We then get

$$\Pi = \frac{(1 + \zeta)\zeta}{\widetilde{D}} - \frac{1}{2}(1 + \zeta^2) + \frac{1}{2}(1 - \zeta^2)\coth\left(\frac{\widetilde{D}}{2}\right). \quad (17)$$

Clearly, compared to the expression in Eq. (15), the effect of this osmotic contribution is to increase the threshold value where repulsion ($\Pi > 0$) can be observed. The two limiting behaviors Eqs. (15) and (17) are sketched in Fig. 5. The corresponding values of the thresholds $\widetilde{D}_0^*$ and $\widetilde{D}_1^*$ are indicated. These two quantities are plotted in Fig. 6 as a function of charge asymmetry, together with the analytical estimation of $\widetilde{D}_1^*$ obtained as follows. If $\widetilde{D}$ is large enough, Eq. (17) simplifies to

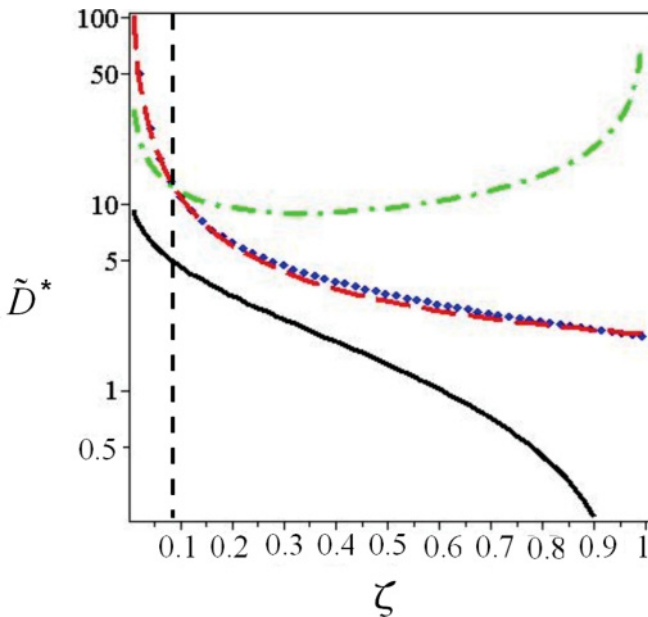$$\Pi \simeq -\zeta^2 + \frac{(1 + \zeta)\zeta}{\widetilde{D}}. \quad (18)$$



FIG. 6. (Color online) Reduced threshold distance discriminating (strong-coupling) attraction from repulsion, as a function of $\zeta$, on a semilogarithmic scale. The solid line shows $\widetilde{D}_0^*$ obtained from Eq. (15); the dotted line is for $\widetilde{D}_1^*$, the exact root of Eq. (17); and the dashed line displays the approximation in Eq. (19). The dot-dashed line shows $\tilde{A}_\perp$, in the particular case $\Xi_2 = 25$: Our approach is meaningful for $\widetilde{D} < \tilde{A}_\perp$ only, which translates into $\zeta > 1/(2\Xi_2 + 1)$ (see the text). Here $1/(2\Xi_2 + 1) \simeq 0.02$.

This expression can now exhibit a repulsive behavior below $\widetilde{D} = (1 + \zeta)/\zeta$, i.e.,

$$D_1^* \simeq \mu_2. \quad (19)$$

It can be seen that this approximation (dashed line) is in fair agreement with the root of Eq. (17) found numerically (dotted line), in the whole available range.

The single-particle picture invoked here relies on two assumptions. First, $\Gamma$ should be large to have pair formation. Second, the (shifted) distance $D$ between the plates should not exceed $A_\perp$ (see the dot-dashed line in Fig. 6). Making use of the approximation in Eq. (19), this means that $1/(2\Xi_2 + 1) < \zeta$. For smaller values of $\zeta$, the analysis is significantly more complex (the single-particle viewpoint is lost). Hence, if $\zeta > 1/(2\Xi_2 + 1)$ the interaction is repulsive at short distances and then turns attractive at intermediate distances, while if $\zeta < 1/(2\Xi_2 + 1)$, Eq. (18) does not lead to any transition between repulsion and attraction and is always repulsive in its range of validity, as is the case for Eq. (11). Of course, for large $\Xi_2$, the threshold $(2\Xi_2 + 1)^{-1}$ is small, so that extremely asymmetric cases only (very low $\zeta$) are not covered by our analysis.

### D. Large separation distances

Our analysis has so far been restricted to short-distance expansions. We are now interested in large-distance asymptotics and in attempting to match the short- and large-distance behaviors. In doing so, we will discuss qualitatively an attraction-repulsion transition of an effective mean-field type, which leads to reentrant attraction as the distance between the two plates is varied from infinity to close contact.

#### 1. Crossover between strong-coupling and mean-field regions for one plate

We will assume first that a given strongly coupled plate (having thus a large $\Xi_i$) can be effectively described by mean-field theory at sufficiently large distances $z$. This common wisdom stems from the remark that for large $z$ the typical distance between counterions becomes large, which leads to a low-coupling regime [24,36,40,41]. It should be emphasized though that the above point of view, which predicts a large-$z$ density decay in $1/z^2$, is incorrect in two dimensions, as shown in a recent work [31]. The present study pertains to three-dimensional systems, so we nevertheless expect for a single plate the crossover scenario discussed in Ref. [41] and summarized in Fig. 7. In essence, the density is expected to decrease exponentially at short distances and algebraically at large distances: Beyond a distance $\delta$ from the plate, the counterion density $n$ is simply given by the solution of the nonlinear Poisson-Boltzmann equation

$$n(\mathfrak{z}) = \frac{1}{2\pi l_B q^2 (\mathfrak{z} + \mu^{\mathrm{eff}})^2}, \quad (20)$$

where $\mathfrak{z} \equiv z - b/2$ and $\mu^{\mathrm{eff}}$ is an effective Gouy-Chapman length characterizing this long-range behavior. Following Ref. [41], one can match the two regimes by assuming that the condensed counterion layer forms a two-dimensional one-component plasma and by applying a mean-field
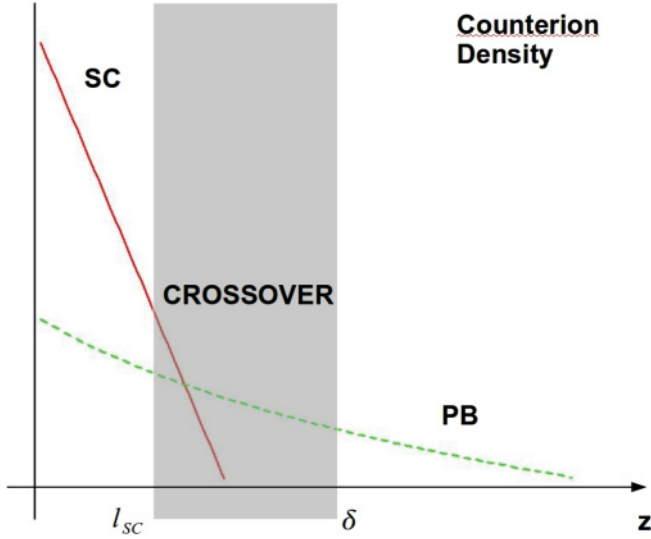
FIG. 7. (Color online) Crossover scheme: following Ref. [41], a schematic representation on a semilogarithmic scale of the crossover between the strong-coupling (SC) and mean-field regimes for the counterion density in the vicinity of a single highly charged plate. The solid curve represents the exponential decay expected close to the plate while the dashed curve stands for the algebraic decay expected at large distances where the Poisson-Boltzmann (PB) theory should hold. The shaded region corresponds to the crossover between these two regimes: $l_{SC}$ is the distance beyond which the exponential decay no longer holds and $\delta$ is the distance to the plate beyond which the PB profile is expected to be valid.

approximation for the dilute layer. Equating the two corresponding chemical potentials yields

$$n(\delta) = n_{SC} e^{-\beta|\varepsilon_c|}, \tag{21}$$

where $n_{SC}$ is a $\delta$-related average density in the condensed layer and $\beta\varepsilon_c(\Xi) \approx -1.56\sqrt{\Xi}$ is the contribution to the two-dimensional one-component plasma chemical potential that stems from the correlations between the counterions [2,24]. Extrapolating the validity of Eq. (20) to $\delta \to b/2$ and assuming that in such a situation $n_{SC}$ is well approximated by the average density over the characteristic length $l_{SC}$, we arrive at [41]

$$n(\mathfrak{z} = 0) = \frac{|\sigma|}{q l_{SC}} (1 - e^{-l_{SC}/\mu}) e^{-1.56\sqrt{\Xi}}. \tag{22}$$

Equation (22) is nothing but the density that the mean-field profile, valid at large distances from the plate, would have if extrapolated at $\mathfrak{z} = 0$ and is therefore not the real density at the plate. However, by invoking Eq. (20), it allows one to estimate the effective Gouy-Chapman length $\mu^{\text{eff}}$ corresponding to the charged plate dressed by a condensed counterion layer, which will prove useful in the following. For the subsequent quantitative discussion, we shall take the value $l_{SC} \approx 3.6\mu$, already used in Ref. [41].

### 2. Application to the two-plate problem

When the separation distance between plates 1 and 2 is decreased from infinity, the first interplate weak-interaction regime is expected to be of mean-field type, so the presumably large-distance attraction may turn into repulsion at a distance

$D_{\text{MF}}^* = |\mu_1^{\text{eff}} - \mu_2^{\text{eff}}|$. In this picture the distance is varied at constant effective Gouy-Chapman lengths $\mu_1^{\text{eff}}$ and $\mu_2^{\text{eff}}$ given by

$$\mu_i^{\text{eff}} = 1.92\mu_i e^{0.78\sqrt{\Xi_i}}, \quad i = 1, 2. \tag{23}$$

If $|\mu_1^{\text{eff}} - \mu_2^{\text{eff}}|$ is significantly larger than the characteristic thresholds obtained in the preceding sections, we should have the reentrant sequence (attraction $\to$ repulsion $\to$ attraction $\to$ repulsion) as $D$ decreases. The first transition is described by a mean-field argument and the last one by strong-coupling considerations, but the intermediate transition (repulsion $\to$ attraction) occurs in a crossover region that resists our theoretical understanding and where additional (repulsion $\to$ attraction) transitions might take place. A related question deals with the lower bound for the distance $D_{\text{bound}}$ below which the mean-field profiles are no longer accurate. For the sake of completeness, we will consider below that $D_{\text{bound}} = a_\perp^{(1)} + a_\perp^{(2)}$. Depending on the respective surface charge densities $\sigma_1$ and $\sigma_2$, we can then discriminate between two distinct situations.

(i) $|\mu_1^{\text{eff}} - \mu_2^{\text{eff}}| < D_{\text{bound}}$. The interaction between the two plates is always attractive at large distances (mean-field regime); at short separation distances, the strong-coupling phenomenology described earlier prevails.

(ii) $|\mu_1^{\text{eff}} - \mu_2^{\text{eff}}| > D_{\text{bound}}$. There is already a transition between attraction and repulsion in the mean-field regime. By decreasing further the distance $D$ and entering the short-distance limit, one should observe another attractive range, as
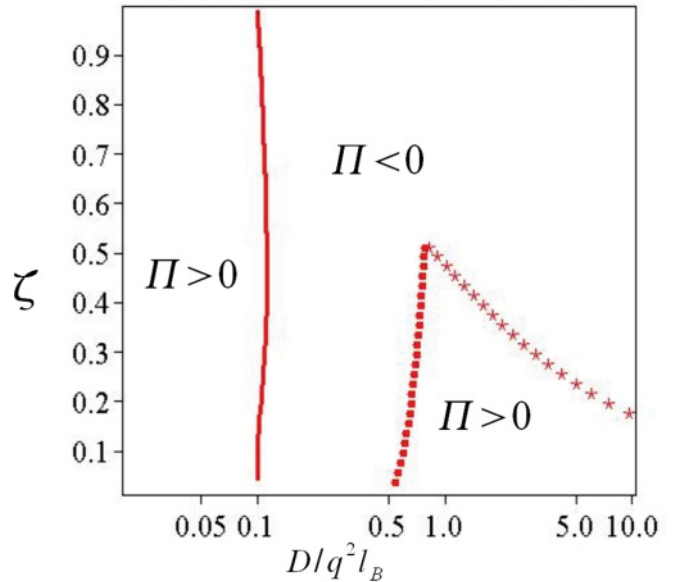


FIG. 8. (Color online) Sketch of attractive and repulsive regimes, as a function of the ratio $\zeta = \sigma_2/|\sigma_1|$ and the distance $D$ (on a logarithmic scale). The repulsive island on the left-hand side, delimited by a continuous line, shows $D_1^*$ where the pressure in Eq. (17) vanishes. The other repulsive region on the right-hand side, delimited by a dotted line (stars), shows $D_{\text{MF}}^* = |\mu_1^{\text{eff}} - \mu_2^{\text{eff}}|$, where the effective Gouy-Chapman lengths are given by Eq. (23). These data are displayed provided that they satisfy the constraint $D_{\text{MF}}^* > D_{\text{bound}} = a_\perp^{(1)} + a_\perp^{(2)}$. Likewise, the left boundary for this mean-field repulsive island has been taken to be $D_{\text{bound}}$, which is shown by a dotted line (squares). Here we have taken $\Xi_2 = 10$.

expressed in Eq. (15) for instance, before repulsion sets in at even smaller separations.

More complicated scenarios could be envisioned, but we summarize in Fig. 8 the simplest possible and provide a phase diagram obtained when considering that the Bjerrum pairs do contribute to the pressure, as in Sec. II C 2. We note that for the parameters chosen there is a reentrant behavior observed with respect to the separation distance, in a large fraction of the $(\zeta, D)$ plane, more specifically, when $\zeta < 0.5$ (this threshold depends on the value of $\Xi_2$ chosen and increases with $\Xi_2$). We recall that the bottom part of the diagram, more specifically, for $\zeta < 1/(2\Xi_2 + 1)$, corresponds to a region where our arguments do not apply, as discussed in Sec. II C 2. In this region our short-scale analysis provides an all-repulsive behavior and we may then speculate that repulsion persists up to the effective mean-field threshold indicated by the asterisks, which corresponds to large distances, on the order of $100 \, q^2 l_B$ or more.

### III. DISCUSSION AND CONCLUSION

In this paper we have analyzed the interaction of two oppositely charged parallel interfaces, each neutralized by its own counterions, without other microions involved (salt-free case, but with two species of microions of opposite signs). We have shown that a repulsive behavior is quite expectedly always present at short enough separations; it simply stems from the diverging entropy cost for confining microions in a slab of vanishing extension. Our analysis completes the known Poisson-Boltzmann phenomenology by investigating the case of strong Coulombic couplings. Short-distance expansions reveal that, depending on the formation of Bjerrum pairs between the oppositely charged microions, an attractive regime may or may not be observed. By formation of pairs we understand here the wealth of different self-assembly scenarios where the pairs may further associate into more complex objects such as chains or various crystals [42,43]. We did not attempt a precise evaluation of the corresponding contribution to the pressure (a particularly demanding task) but rather we analyzed limiting cases where this unknown contribution is bounded by reasonable values (see Sec. II C). We have supplemented our short-distance analysis by a more speculative investigation of the large-distance behavior, from which a phase diagram was put forth with reentrant features between attraction and repulsion as the distance $D$ between the plates is varied. The experimental observation of such features would imply that other sorts of interactions, such as van der Waals, do not modify the main effects uncovered.

In our approach single-particle arguments play a crucial role and allow us to compute the density of microions from which the equation of state follows. These single-particle arguments, however, are *a priori* not restricted to strongly

coupled interfaces, but can equally be invoked when the coupling parameters $\Xi_1$ and $\Xi_2$ are small (see, e.g., Sec. 3.3 of Ref. [44] and in particular Fig. 16 therein for simulation results backing up this statement in the like-charge case $\sigma_1 = \sigma_2$). Indeed, when $D$ becomes smaller than the characteristic lateral distance $a_\perp$ between ions, these ions effectively decouple and experience the external potential of the plates only (we are concerned here with the ionic density dependence on the $z$ coordinate, perpendicular to the plate; in the transverse direction, parallel to the plate, a correlation hole remains around each particle, of typical size $q^2 l_B$). As a consequence, the pressures given by Eqs. (11), (15), and (17) still hold with the same range of validity for $\Xi_i \to 0$. In the corresponding distance range, the Poisson-Boltzmann results break down due to discreteness effects. (It is therefore essential here to make a clear distinction between Poisson-Boltzmann theory and the low-$\Xi$ limit of the original model dealing with discrete particles: The Poisson-Boltzmann approach considers from the outset continuous density fields and therefore cannot be expected to hold at separation distances such that discreteness effects do matter, i.e., when $D < a_\perp$; the adequacy of the Poisson-Boltzmann approach to describe the low-$\Xi$ physics should then be understood as a statement that excludes a small range of short separations $D$.) From the analysis of Sec. II we learn that when Bjerrum pair formation can be neglected, the threshold distance $D^*$ where repulsive behavior sets in is still given by the Poisson-Boltzmann result $|\mu_2 - \mu_1| = \mu_2 - \mu_1$ provided this length is larger than both characteristic distances $a_\perp^{(1)}$ and $a_\perp^{(2)}$. In the opposite case, when $|\mu_2 - \mu_1| < \inf(a_\perp^{(1)}, a_\perp^{(2)})$, we may speculate that $D^*$ lies between $a_\perp^{(1)}$ and $a_\perp^{(2)}$ since the single-particle argument that holds at smaller separations leads to repulsion, while the Poisson-Boltzmann theory yields attraction at larger separations [20]. If, in contrast, Bjerrum pairs form and contribute to the pressure through their mean density (see Sec. II C 2), we have seen that $D^* = \mu_2$, which is thus larger than the Poisson-Boltzmann result $\mu_2 - \mu_1$. However, this result only holds provided $\zeta > (1 + 2\Xi_2)^{-1} \simeq 1$ (we are still considering the low-$\Xi_i$ limit). Given that $\zeta \leqslant 1$ by definition (i.e., $\sigma_2 < |\sigma_1|$), we see that here the single-particle picture does not apply up to $\mu_2$ (except in a small-$\zeta$ region close to 1), which means that $D^*$ is larger than $A_\perp = [\pi(|\sigma_1| - \sigma_2)]^{-1/2}$. It can be checked that, generically, this length is smaller than the Poisson-Boltzmann prediction $\mu_2 - \mu_1$, except again in a small-$\zeta$ region around unity.

[1] J.-P. Hansen and H. Löwen, Annu. Rev. Phys. Chem. **51**, 209 (2000).

[2] Y. Levin, Rep. Prog. Phys. **65**, 1577 (2002).

[3] R. Messina, J. Phys. Condens. Matter **21**, 113102 (2009).

[4] N. Ben-Tal, J. Phys. Chem. **99**, 9642 (1995).

[5] J. Z. Wu, D. Bratko, H. W. Blanch, and J. M. Prausnitz, Phys. Rev. E **62**, 5273 (2000).

[6] E. J. Tull, P. Bartlett, and K. R. Ryan, Langmuir **23**, 7859 (2007).

[7] J. Jens Rydén, M. Ullner, and P. Linse, J. Chem. Phys. **123**, 034909 (2005).

[8] V. Dahirel and J.-P. Hansen, J. Chem. Phys. **131**, 084902 (2009).

[9] B. Jonsson and J. Stahlberg, Colloid. Surf. B **14**, 67 (1999).

[10] S. Bigdeli, A. H. Talasaz, P. Stahl, H. Persson, M. Ronaghi, R. W. Davis, and M. Nemat-Gorgani, Biotechnol. Bioeng. **100**, 19 (2008).

[11] J.-R. Morones *et al.*, Nanotechnology **16**, 2346 (2005).

[12] S. Jones, H. Shanahan, H. Berman, and J. Thornton, Nucleic Acids Res. **31**, 7189 (2003).

[13] J. Vervey and J. T. G. Overbeek, *Theory of the Stability of Lyophobic Colloïds* (Elsevier, Amsterdam, 1948).

[14] S. Bhattacharjee and M. Elimelech, J. Colloid Interface Sci. **193**, 273 (1997).

[15] V. A. Parsegian and D. Gingell, Biophys. J. **12**, 1192 (1972).

[16] H. Ohshima, Colloid Polym. Sci. **253**, 150 (1975).

[17] P. Sens and J.-F. Joanny, Phys. Rev. Lett. **84**, 4862 (2000).

[18] D. Ben-Yaakov, Y. Burak, D. Andelman, and S. Safran, Europhys. Lett. **79**, 48002 (2007).

[19] F. Paillusson, M. Barbi, and J.-M. Victor, Mol. Phys. **107**, 1379 (2009).

[20] V. Dahirel, F. Paillusson, M. Jardat, M. Barbi, and J.-M. Victor, Phys. Rev. Lett. **102**, 228101 (2009).

[21] R. Netz, Eur. Phys. J. E **5**, 557 (2001).

[22] A. Naji, S. Jungblut, A. Moreira, and R. Netz, Physica A **352**, 131 (2005).

[23] I. Rouzina and V. Bloomfield, J. Phys. Chem. **100**, 9977 (1996).

[24] B. I. Shklovskii, Phys. Rev. E **60**, 5802 (1999).

[25] M. Kanduč, M. Trulsson, A. Naji, Y. Burak, J. Forsman, and R. Podgornik, Phys. Rev. E **78**, 061105 (2008).

[26] Y. S. Jho, M. Kanduč, A. Naji, R. Podgornik, M. W. Kim, and P. A. Pincus, Phys. Rev. Lett. **101**, 188101 (2008).

[27] D. Dean, R. Horgan, A. Naji, and R. Podgornik, J. Chem. Phys. **130**, 094504 (2009).

[28] M. Kanduč, A. Naji, J. Forsman, and R. Podgornik, J. Chem. Phys. **132**, 124701 (2010).

[29] M. Hatlo and L. Lue, EPL **89**, 25002 (2010).

[30] M. Kanduč, A. Naji, J. Forsman, and R. Podgornik, Phys. Rev. E **84**, 011502 (2011).

[31] L. Šamaj and E. Trizac, Eur. Phys. J. E **34**, 20 (2011).

[32] L. Šamaj and E. Trizac, Phys. Rev. Lett. **106**, 078301 (2011).

[33] D. Henderson and L. Blum, J. Chem. Phys. **69**, 5441 (1978).

[34] H. Wennerström, B. Jönsson, and P. Linse, J. Chem. Phys. **76**, 4665 (1982).

[35] J. Zwanikken and R. van Roij, J. Phys. Condens. Matter **21**, 424102 (2009).

[36] Y. Burak, D. Andelman, and H. Orland, Phys. Rev. E **70**, 016102 (2004).

[37] Y.-G. Chen and J. Weeks, Proc. Natl. Acad. Sci. USA **103**, 7560 (2006).

[38] C. D. Santangelo, Phys. Rev. E **73**, 041512 (2006).

[39] S. Buyukdagli, M. Manghi, and J. Palmeri, Phys. Rev. Lett. **105**, 158103 (2010).

[40] H. Boroudjerdi, Y.-W. Kim, A. Naji, R. Netz, X. Schlagberger, and A. Serr, Phys. Rep. **416**, 129 (2005).

[41] A. dos Santos, A. Diehl, and Y. Levin, J. Chem. Phys. **130**, 124110 (2009).

[42] J. J. Weis and D. Levesque, Phys. Rev. Lett. **71**, 2729 (1993).

[43] L. Assoud, R. Messina, and H. Löwen, Europhys. Lett. **89**, 36001 (2010).

[44] A. G. Moreira and R. R. Netz, Eur. Phys. J. E **8**, 33 (2002).